





RESEARCH PAPER

# New opportunities and insights into *Papaver* self-incompatibility by imaging engineered *Arabidopsis* pollen

Ludi Wang<sup>1</sup>, Marina Triviño<sup>1,2,3</sup>, Zongcheng Lin<sup>2,3</sup>, José Carli<sup>1</sup>, Deborah J. Eaves<sup>4</sup>, Daniël Van Damme<sup>2,3</sup>, Moritz K. Nowack<sup>2,3</sup>, , Vernonica E. Franklin-Tong<sup>4,\*</sup> and Maurice Bosch<sup>1,\*</sup> 

<sup>1</sup> Institute of Biological, Environmental and Rural Sciences (IBERS), Aberystwyth University, Plas Gogerddan, Aberystwyth SY23 3EE, UK

<sup>2</sup> Department of Plant Biotechnology and Genetics, Ghent University, 9052 Ghent, Belgium

<sup>3</sup> VIB Center for Plant Systems Biology, 9052 Ghent, Belgium

<sup>4</sup> School of Biosciences, College of Life and Environmental Sciences, University of Birmingham, Edgbaston, Birmingham B15 2TT, UK

\* Correspondence: [v.e.franklin\\_tong@bham.ac.uk](mailto:v.e.franklin_tong@bham.ac.uk) or [mub@aber.ac.uk](mailto:mub@aber.ac.uk)

Received 5 November 2019; Editorial decision 7 February 2020; Accepted 25 February 2020

Editor: Zoe Wilson, University of Nottingham, UK

## Abstract

Pollen tube growth is essential for plant reproduction. Their rapid extension using polarized tip growth provides an exciting system for studying this specialized type of growth. Self-incompatibility (SI) is a genetically controlled mechanism to prevent self-fertilization. Mechanistically, one of the best-studied SI systems is that of *Papaver rhoeas* (poppy). This utilizes two S-determinants: stigma-expressed PrsS and pollen-expressed PrpS. Interaction of cognate PrpS–PrsS triggers a signalling network, causing rapid growth arrest and programmed cell death (PCD) in incompatible pollen. We previously demonstrated that transgenic *Arabidopsis thaliana* pollen expressing PrpS–green fluorescent protein (GFP) can respond to *Papaver* PrsS with remarkably similar responses to those observed in incompatible *Papaver* pollen. Here we describe recent advances using these transgenic plants combined with genetically encoded fluorescent probes to monitor SI-induced cellular alterations, including cytosolic calcium, pH, the actin cytoskeleton, clathrin-mediated endocytosis (CME), and the vacuole. This approach has allowed us to study the SI response in depth, using multiparameter live-cell imaging approaches that were not possible in *Papaver*. This lays the foundations for new opportunities to elucidate key mechanisms involved in SI. Here we establish that CME is disrupted in self-incompatible pollen. Moreover, we reveal new detailed information about F-actin remodelling in pollen tubes after SI.

**Keywords:** Actin, actin-binding proteins (ABPs), calcium, endocytosis, fluorescent probes, programmed cell death (PCD), pH, pollen tube growth, live-cell imaging, self-incompatibility (SI).

## Introduction

Pollination in higher plants is a crucial event, required for fertilization and seed set. The acceptance of compatible pollen and the subsequent steps leading to successful fertilization comprise a complex series of events involving interaction between the pollen and pistil (see Dresselhaus and Franklin-Tong, 2013). A compatible pollen grain landing on a stigma adheres and hydrates; if this is successful, it germinates and a

pollen tube emerges. The pollen tube grows using polar tip growth to navigate its way to the ovules, interacting with the maternal reproductive tissues of the pistil, and transports the sperm cells to the ovules, where they effect fertilization. Over the last decade or so, our knowledge of molecular components involved in the interactions between pollen and pistil during both compatible and incompatible pollinations

has increased extensively (see the recent review by [Bedinger \*et al.\*, 2017](#)).

Pollen tubes extend extremely rapidly (up to  $1 \text{ cm h}^{-1}$  in maize; [Barnanas and Fridvalszky, 1984](#)), providing a wonderful system to study this specialized type of cellular growth ([Qin and Yang, 2011](#)). Tip growth depends on polar exocytosis to deliver plasma membrane and cell wall material to the apical region ([Hepler \*et al.\*, 2001](#); [Yang, 2008](#); [Luo \*et al.\*, 2017](#)), and on clathrin-mediated endocytosis (CME), which internalizes excess membrane material deposited by exocytosis at the pollen tube tip ([Grebnev \*et al.\*, 2017](#); [Zhang \*et al.\*, 2019](#)). Pollen grains can germinate to produce pollen tubes *in vitro*, providing a great experimental system to study the control of tip growth, without the complication of pistil tissues. Unlike most plant cells, which dedifferentiate and lose polarity when put into *in vitro* culture, pollen maintains its identity and polarity. While they do not grow to the lengths observed *in vivo*, *in vitro* grown pollen tubes grow relatively uniformly and exhibit highly polarized cytoplasmic organization with several zones, including an apical zone packed with vesicles, a cytoplasmic-rich nuclear zone, and a vacuolar zone further back ([Hepler \*et al.\*, 2001](#)). Cytoplasmic streaming moves organelles in a reverse fountain pattern and depends on an intact actin cytoskeleton ([Staiger \*et al.\*, 2010](#)). The accumulated knowledge so far reveals the existence of a complex, self-organizing signalling network, utilizing, amongst others, a tip-localized Rho GTPase, apical cytosolic  $\text{Ca}^{2+}$  gradients, reactive oxygen species (ROS), the actin cytoskeleton, and vesicular trafficking to supply cell wall and membrane components for pollen tube growth (see [Qin and Yang, 2011](#) for a review).

In addition to mechanisms to maximize reproductive success, many higher plants utilize mechanisms to avoid self-fertilization. Self-incompatibility (SI) is the main genetic mechanism to prevent inbreeding. It is specified by *S*-determinant genes at a highly polymorphic, multiallelic *S*-locus; see [Fujii \*et al.\*, 2016](#)). Here we describe the SI system in *Papaver rhoeas*, which has been well characterized, especially with respect to the downstream events triggered by the *S*-specific interaction (see reviews by [Wilkins \*et al.\*, 2014](#); [Wang \*et al.\*, 2019](#)). SI in *Papaver* utilizes two genetically linked *S*-determinants: a pollen-expressed transmembrane protein, PrpS, and a stigma-expressed secreted protein, PrsS. Interaction of cognate PrpS–PrsS results in rejection of incompatible pollen, triggering a signalling network causing rapid growth arrest and ensuing programmed cell death (PCD) in incompatible pollen. This SI system serves as a good model system to investigate various ways in which pollen tube tip growth can be prevented, thereby providing insights into mechanisms involved in regulating pollen tube growth. Below we describe in more detail key features of the *Papaver* SI system that are relevant to the current study.

A key feature of *Papaver* SI is the inhibition of pollen tube growth. One of the first events observed after a cognate PrpS–PrsS interaction is a loss of the apically focused gradient of cytosolic free  $\text{Ca}^{2+}$  ( $[\text{Ca}^{2+}]_{\text{cyt}}$ ), typical of growing pollen tubes ([Hepler \*et al.\*, 2001](#)), and a concomitant rapid increase in  $[\text{Ca}^{2+}]_{\text{cyt}}$  in the shank of the pollen tube ([Franklin-Tong \*et al.\*, 1993, 1995, 1997](#)). More recently, evidence for  $\text{Ca}^{2+}$  influx has been obtained ([Wu \*et al.\*, 2011](#)). Downstream, SI triggers rapid

increases in ROS in the pollen tube shank ([Wilkins \*et al.\*, 2011, 2014](#)). SI also triggers dramatic acidification of the cytosol ( $[\text{pH}]_{\text{cyt}}$ ), with the pH dropping rapidly to 6.5 within 10 min, reaching pH 5.5 by ~60 min ([Wilkins \*et al.\*, 2015](#)).

However, *Papaver* SI does not end with just inhibition of pollen tube growth. The SI-induced signalling cascade also triggers PCD involving a DEVDase/caspase-3-like activity that is activated several hours after the initial cognate interaction ([Thomas and Franklin-Tong, 2004](#); [Bosch and Franklin-Tong, 2007](#)). This enzyme has a pH optimum of ~5.5 and is inactive at normal physiological pH of ~6.8 ([Bosch and Franklin-Tong, 2007](#); [Wilkins \*et al.\*, 2015](#)). The cytosolic acidification induced by SI fits well with the optimal activity of this caspase-like enzyme. Indeed, data have shown that cytosolic acidification is necessary and sufficient to trigger PCD in *Papaver* pollen tubes ([Wilkins \*et al.\*, 2015](#)), suggesting that this is an important decision-making step in SI-PCD.

The actin cytoskeleton, which plays a key role in many cellular events, including tip growth, morphogenesis, and vesicle trafficking, is a key target of SI in *Papaver*. A cognate PrpS–PrsS interaction triggers rapid actin depolymerization, sufficient to inhibit pollen tube growth, which relies on an intact F-actin network ([Snowman \*et al.\*, 2002](#)). Downstream of this SI-induced actin depolymerization, further major alterations in actin localization and dynamics are observed, involving the formation of ‘punctate foci’; these are unusually stable actin structures and are a key feature of SI pollen ([Poulter \*et al.\*, 2010](#)). SI-induced acidification plays a key role in mediating actin remodelling. Artificial manipulation of the  $[\text{pH}]_{\text{cyt}}$  of pollen tubes revealed that pH 5.5 triggered the formation of numerous F-actin foci, while buffering to pH 7, to prevent SI-induced acidification, blocked the formation of these actin foci ([Wilkins \*et al.\*, 2015](#)). This demonstrated that acidification was required for these actin alterations. Studies in other eukaryotic cells have shown that changes in cytoskeletal dynamics can influence whether PCD is initiated (see reviews by [Franklin-Tong and Gourlay, 2008](#); [Smertenko and Franklin-Tong, 2011](#)). In *Papaver*, experiments using actin depolymerization and stabilization treatments implicated that both types of actin alterations can trigger a caspase-3 like/DEVDase activity. This, together with other data, provided evidence that actin alterations are implicated in not only inhibition of pollen tube growth, but also in mediating PCD ([Thomas \*et al.\*, 2006](#); [Bosch and Franklin-Tong, 2008](#)).

Actin-binding proteins (ABPs) regulate virtually every aspect of the actin cytoskeleton, including its assembly, turnover, dynamics, and organization ([Staiger \*et al.\*, 2010](#); [Pollard, 2016](#)). In incompatible *Papaver* pollen, the SI-induced actin foci are associated with at least two ABPs: actin-depolymerizing factor (ADF/cofilin) and cyclase-associated protein (CAP/Srv2p; [Poulter \*et al.\*, 2010](#)), suggesting their involvement in the formation of these highly stable F-actin foci observed during SI in incompatible pollen.

Recent studies have demonstrated the functional transfer of PrpS and PrsS to *Arabidopsis thaliana*, rendering these plants fully self-incompatible, with little or no seed set ([Lin \*et al.\*, 2015](#)), despite *Arabidopsis* being highly diverged (>140 million years) from *Papaver*. A previous study showed that addition

of recombinant PrsS to *Arabidopsis* pollen expressing PrpS resulted in key features of the *Papaver* pollen SI response, including formation of actin foci and increases in DEVDase/caspase-3-like activity (de Graaf *et al.*, 2012). These data suggested that *Arabidopsis* pollen has the cellular machinery required for the activation of downstream events triggered by PrpS–PrsS interaction. The successful functional transfer of the *Papaver* SI system to *Arabidopsis* (de Graaf *et al.*, 2012; Lin *et al.*, 2015) provides exciting opportunities to further dissect the SI-induced signalling networks and events leading to PCD in this model system. Here we describe recent advances in utilizing the engineered *Arabidopsis* ‘SI’ system in combination with a range of genetically encoded probes that allows us to study the mechanistic basis of the *Papaver* SI-PCD system in depth. This provides new opportunities and directions to further elucidate and dissect key mechanisms and components involved in SI-PCD.

## Materials and methods

### Plant material and growth conditions

*Arabidopsis thaliana* accession Columbia-0 (Col-0) seeds and those from derived transgenic lines were grown at 22 °C in a 16 h light/8 h dark cycle. Pollen grains from mature flowers of the marker lines were used (see Supplementary Table S1 and Supplementary Fig. S1 at JXB online).

### Growth of *Arabidopsis* pollen tubes and treatments

*Arabidopsis* pollen was hydrated for 50 min in 35 mm glass-bottom microwell culture dishes with a 10 mm No. 1.5 coverglass (MatTek Corp.) coated with 0.01% (w/v) poly-L-lysine. Hydrated pollen was grown in liquid germination medium (GM) comprising 15% (w/v) sucrose, 0.01% (w/v) H<sub>3</sub>BO<sub>3</sub>, 5 mM KCl, 1 mM MgSO<sub>4</sub>, 2.5 mM CaCl<sub>2</sub>, and 2.5 mM Ca(NO<sub>3</sub>)<sub>2</sub> (modified from de Graaf *et al.*, 2012) for >60 min prior to treatment. Recombinant PrsS<sub>1</sub> proteins were produced as described previously (Wilkins *et al.*, 2015). SI was induced by adding recombinant PrsS<sub>1</sub> with a final concentration of 20 µg ml<sup>-1</sup>. Controls were treated with GM or heat-inactivated PrsS<sub>1</sub>. Manipulation of cytosolic pH was achieved as described by Wilkins *et al.* (2015). PrsS<sub>1</sub> and the Ac-DEVD-AMC probe (1.5 mM final concentration) were simultaneously added. For treatments that included Ac-DEVD-CHO (100 µM final concentration), this was added at the same time as PrsS<sub>1</sub> and Ac-DEVD-AMC.

### In vitro test of PrsS<sub>1</sub> activity

Pollen tubes were grown and treated as described above. Pollen tubes were imaged immediately after, and 2 h after SI treatment, using a Leica DMi8 microscope equipped with a Leica TCS SPE camera. Pollen tube lengths [20 pollen tubes per treatment for each experiment, three independent experiments (*n*=60 for each treatment)] were measured using Fiji software (Schindelin *et al.*, 2012).

### Reverse transcription–PCR analysis of PrpS<sub>1</sub> expression level in *Arabidopsis* lines

PrpS<sub>1</sub> expression in *Arabidopsis* pollen from transgenic PrpS<sub>1</sub>–green fluorescent protein (GFP), YC3.6–PrpS<sub>1</sub>, pHGFP–PrpS<sub>1</sub>, and PrpS<sub>1</sub> lines was analysed using reverse transcription–PCR (RT–PCR) on cDNA prepared from mature flowers. Total RNA was extracted using TRIzol reagent (Life Technologies) and purified using RNeasy MiniElute Cleanup Kit columns (Qiagen). After DNase I treatment (New England Biolabs), isolated total RNA was used for cDNA synthesis (SuperScript<sup>®</sup> III First-Strand Synthesis System, Life Technologies) followed by PCR using PrpS<sub>1</sub> gene-specific primers (see Supplementary Table S2).

Glyceraldehyde-3-phosphate dehydrogenase (GAPD) primers were used as a positive control.

### FM4-64 internalization assays

FM4-64 was added to pollen tubes expressing PrpS<sub>1</sub>–GFP at different time points after SI induction to a final concentration of 3 µM and incubated for 20 min prior to imaging. The FM4-64 signal was observed with a Leica SP8 confocal microscope equipped with a ×100 CS2 oil objective (NA 1.40, excitation 561 nm, emission 600–680 nm). FM4-64 signal intensity was measured using Fiji. Regions of interest (ROIs) were selected based on the plasma membrane or cytosol area 15–25 µm from the apex.

### Visualization of TPLATE–TagRFP, TPLATE–GFP, and CLC2–TagRFP

Pollen tubes from plants harbouring *pLAT52::TPLATE-TagRFP\_pNTP303::PrpS<sub>1</sub>-GFP* (homozygous *tplate/tplate* background) and *pLAT52::TPLATE-GFP (tplate/tplate)\_pRPS5A::CLC2(At2g40060)-TagRFP* (Supplementary Table S1A; Gadeyne *et al.*, 2014; see Supplementary Protocols) were observed using a Leica SP8 confocal microscope (×100 CS2 objective, NA 1.40); red fluorescent protein (RFP) excitation 561 nm, emission 571–700 nm; GFP excitation 488 nm. Fluorescence intensity was obtained using the standard profiling function in Fiji.

### Ratio-imaging of cytosolic Ca<sup>2+</sup>

Pollen tube [Ca<sup>2+</sup>]<sub>cyt</sub> was imaged using a Leica SP8 confocal microscope (×100 CS2 objective, NA 1.40). The YC3.6 Ca<sup>2+</sup> sensor (Nagai *et al.*, 2004) was excited at 458 nm; emissions of cyan fluorescent protein (CFP; 465–500 nm) and Venus (520–570 nm) were collected simultaneously. Images were processed using Leica Application Suite X (LAS X).

### Visualization and image analyses of F-actin

Lifeact–mRuby2 (Riedl *et al.*, 2008; Bascom *et al.*, 2018) was used to visualize the F-actin cytoskeleton. For the ‘slow’ SI line, Lifeact–mRuby2 was introduced by transformation of *pNTP303::Lifeact-mRuby2* into *Arabidopsis* plants harbouring *pNTP303::PrpS<sub>1</sub>-GFP* as described previously (de Graaf *et al.*, 2012). For the ‘fast’ lines, Lifeact–mRuby2 was introduced by crossing *Arabidopsis* plants expressing Lifeact–mRuby2 with lines harbouring *pNTP303::YC3.6-pNTP303::PrpS<sub>1</sub>* or *pNTP303::pHGFP-pNTP303::PrpS<sub>1</sub>* (Table S1). F-actin labelled with Lifeact–mRuby2 was observed using a Leica SP8 confocal microscope (×100 CS2 objective, NA 1.40, excitation 561 nm). A kymograph with a line thickness of 1 pixel along the area adjacent to the plasma membrane of pollen tubes was generated to analyse the intensity of F-actin at the pollen tube cortex and pseudocolour-processed using Fiji (Schindelin *et al.*, 2012). The distribution of F-actin filament orientation was analysed by using the ImageJ/Fiji plugin ‘OrientationJ’ (Rezakhaniha *et al.*, 2012; Püspöki *et al.*, 2016).

### Ratio-imaging of pHGFP

The cytosolic pH sensor pHGFP was sequentially excited at 405 nm and 488 nm. For each of the excitations, the emission was collected separately between 500 nm and 530 nm. Using LAS X software, the fluorescent intensity ratios from the 405 nm and 488 nm excitation channels (R<sub>405/488</sub>) were quantified in an ROI of 5×20 µm covering an area 15–35 µm distal from the apex. A standard curve defining pH values relative to the R<sub>405/488</sub> was generated after each imaging session by measuring R<sub>405/488</sub> in pollen tubes treated with 50 mM propionic acid pH 7.5, 7.0, 6.5, 6.0, and 5.5, respectively.

### Analysis of vacuolar morphology

Pollen grains expressing PrpS<sub>1</sub>–GFP and the tonoplast fluorescent marker WAVE9R, containing mCherry attached to VAMP711 (Geldner *et al.*, 2009; Supplementary Table S1), were analysed for vacuolar



morphology. Arabidopsis lines carrying both *pNTP303::PrpS<sub>1</sub>-GFP* and *pUBQ10::VAMP711-mCherry* were obtained by crossing and selection of lines positive for both cassettes. Mid-plane images of pollen tubes were acquired using a Leica SP8 confocal microscope (×63 CS2 objective, NA 1.20, excitation 561 nm, emission 576–680 nm).

### Analysis of PCD

The fluorescent probe Ac-DEVD-AMC was used for the detection of SI-induced DEVDase activity in pollen grains expressing PrpS<sub>1</sub>. Pollen samples were incubated in the dark and images were taken every 30 min using a Leica SP8 confocal microscope (×63 CS2 objective, NA 1.20, excitation 405 nm, emission 451–496 nm). For each time point, 100–300 pollen grains were scored in three independent experiments. The AMC signal was quantified using LAS X software, based on the mean fluorescence intensity values from a 15 µm diameter ROI, drawn over individual pollen grains. *P*-values were calculated using the Wilcoxon test. Nuclear disruption was assessed using Arabidopsis pollen expressing PrpS<sub>1</sub>-GFP and NLS (nuclear localization signal)-tdTomato (Supplementary Table S1); ×63 CS2 objective, NA 1.20, excitation 561 nm, emission 596–665 nm.

## Results

### PrpS-PrpS interaction triggers inhibition of Arabidopsis pollen tube growth

Pollen tubes from the engineered Arabidopsis ‘SI’ system plants were grown *in vitro* and either recombinant PrpS proteins were added to stimulate SI or GM was added as a control (see the Materials and methods; Fig. 1A). These *in vitro* assays confirmed the S-specific activity of PrpS<sub>1</sub>, as pollen tube growth rates were significantly inhibited when

recombinant PrpS<sub>1</sub> was added to pollen tubes expressing PrpS<sub>1</sub>-GFP (a cognate combination triggering SI, Fig. 1B; Supplementary Movie S1). No growth inhibition was observed for wild-type pollen tubes treated with GM or PrpS<sub>1</sub>. Likewise, pollen tubes expressing PrpS<sub>3</sub>-GFP treated with PrpS<sub>1</sub> (a compatible combination) were not inhibited. These data correspond to the previously reported SI response in PrpS-expressing Arabidopsis pollen (de Graaf et al., 2012), and serve as a baseline to confirm the biological activity of PrpS<sub>1</sub> and the S-specific incompatible response triggered. Arabidopsis lines expressing PrpS together with various fluorescent genetic markers varied in their responses. Semi-quantitative RT-PCR analysis of the lines (Supplementary Table S1) linked this variation with differences in PrpS<sub>1</sub> expression levels in these lines (Fig. 1C); we will describe the effect of this later.

### PrpS-PrpS interaction triggers alterations in clathrin-mediated endocytosis

CME is important in mediating pollen tube growth (Grebnev et al., 2017). However, whether SI affects pollen tube membrane internalization has not previously been established. To monitor the dynamics of CME during the SI response, we visualized CME by using the internalization of the endocytic tracer dye FM4-64 as a readout of altered endocytosis, and TPLATE, as a member of the endocytic TPLATE complex (TPC), as an indicator for CME (Gadeyne et al., 2014). The uptake of FM4-64 into pollen tubes was significantly inhibited within 5 min after SI induction (Fig. 2A), which provides

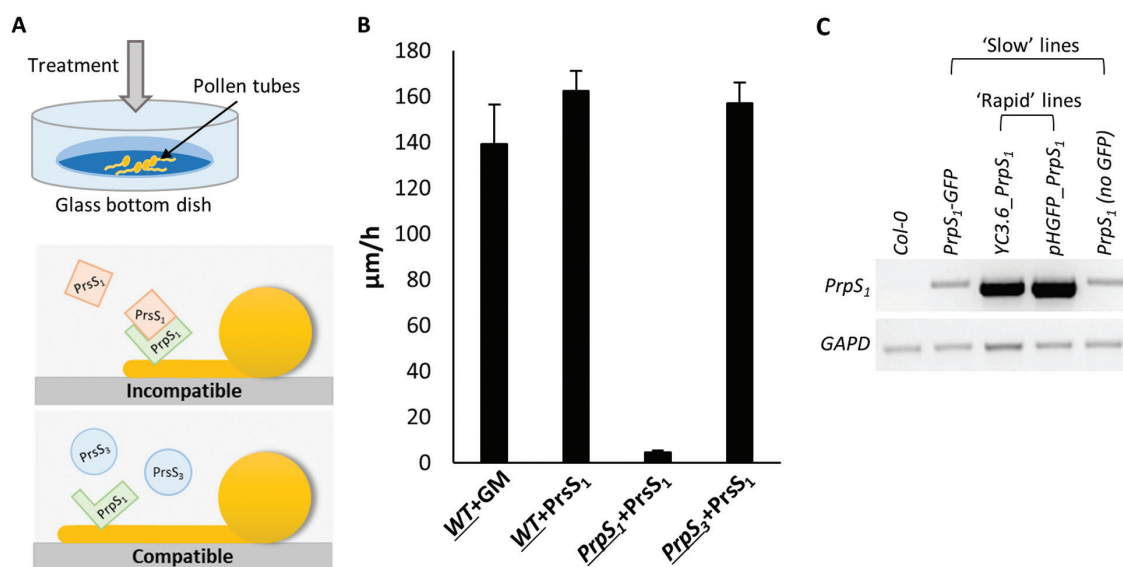


**Fig. 1.** S-specific inhibition of *in vitro* growth of transgenic Arabidopsis pollen tubes undergoing an incompatible response. (A) Cartoon illustrating the *in vitro* pollen tube growth system in liquid germination medium (GM). Treatment of a transgenic Arabidopsis pollen tube expressing PrpS<sub>1</sub> with recombinant PrpS<sub>1</sub> triggers inhibition, as it is an incompatible combination, but when PrpS<sub>3</sub> is added to a pollen tube expressing PrpS<sub>1</sub> (a compatible combination), pollen tube growth is not inhibited. (B) *In vitro* growth rates of pollen tubes. Wild-type (WT) pollen tubes treated with GM or recombinant PrpS<sub>1</sub> have normal growth rates; pollen tubes expressing PrpS<sub>3</sub> treated with recombinant PrpS<sub>1</sub> are compatible and display normal growth rates; pollen tubes expressing PrpS<sub>1</sub> treated with recombinant PrpS<sub>1</sub> are incompatible and pollen tube growth is arrested (*n*=60). The pollen genotype is underlined. (C) Semi-quantitative RT-PCR shows the different expression levels of PrpS<sub>1</sub> in transgenic *A. thaliana* lines harbouring constructs containing PrpS<sub>1</sub> used in this study. GAPD was used as an internal control. ‘Slow’ and ‘rapid’ refer to the speed of the SI response associated with low and high PrpS<sub>1</sub> expression levels, respectively.

evidence that endocytosis is inhibited very early during the SI response. This block in internalization thus occurs concomitantly with SI-induced inhibition of pollen tube growth.

TPLATE is one of the eight subunits of TPC, which functions as a crucial plasma membrane-localized adaptor complex for CME in plants (Van Damme *et al.*, 2011; Gadeyne *et al.*, 2014). Similar to what has been shown for TPLATE-GFP (Van Damme *et al.*, 2006), TPLATE-TagRFP is recruited to the plasma membrane in the subapical area of growing pollen tubes (Fig. 2B; Supplementary Fig. S2). This localization of TPLATE is in agreement with observations of another TPC subunit, TML, identifying the subapical plasma membrane region as the site of CME during pollen tube growth (Gadeyne *et al.*, 2014). Within 2 min after SI induction, TPLATE no longer localized at the plasma membrane (Fig. 2C, D). These results provide evidence that CME is rapidly inhibited early during the SI response.

As CME dynamics in Arabidopsis depend on cytoplasmic pH (Dejonghe *et al.*, 2016), this suggested that SI-induced cytosolic acidification (Wilkins *et al.*, 2015; Fig. 5) may affect

CME in pollen tubes. To investigate the effect of low cytosolic pH on CME in pollen tubes, we used propionic acid to manipulate pollen tube  $[pH]_{\text{cyt}}$  (Wilkins *et al.*, 2015). TPLATE-GFP and CLC2-TagRFP (Gadeyne *et al.*, 2014) maintained their localization at the plasma membrane of the subapical area of pollen tubes with propionic acid pH 7.0 (Fig. 2E, F). The recruitment of TPLATE-GFP and CLC2-mTagRFP at the plasma membrane was disrupted by the addition of propionic acid pH 5.5 (Fig. 2E, F). As a functional TPC, together with CLC2 at the plasma membrane, is required for CME (Van Damme *et al.*, 2011; Gadeyne *et al.*, 2014), our observations suggest that CME is altered and inhibited by acidic cytosolic conditions.

### *PrsS-PrpS interaction triggers increases in cytosolic $Ca^{2+}$*

To determine whether PrpS-expressing Arabidopsis pollen tubes undergo similar  $[Ca^{2+}]_{\text{cyt}}$  alterations to *Papaver* pollen

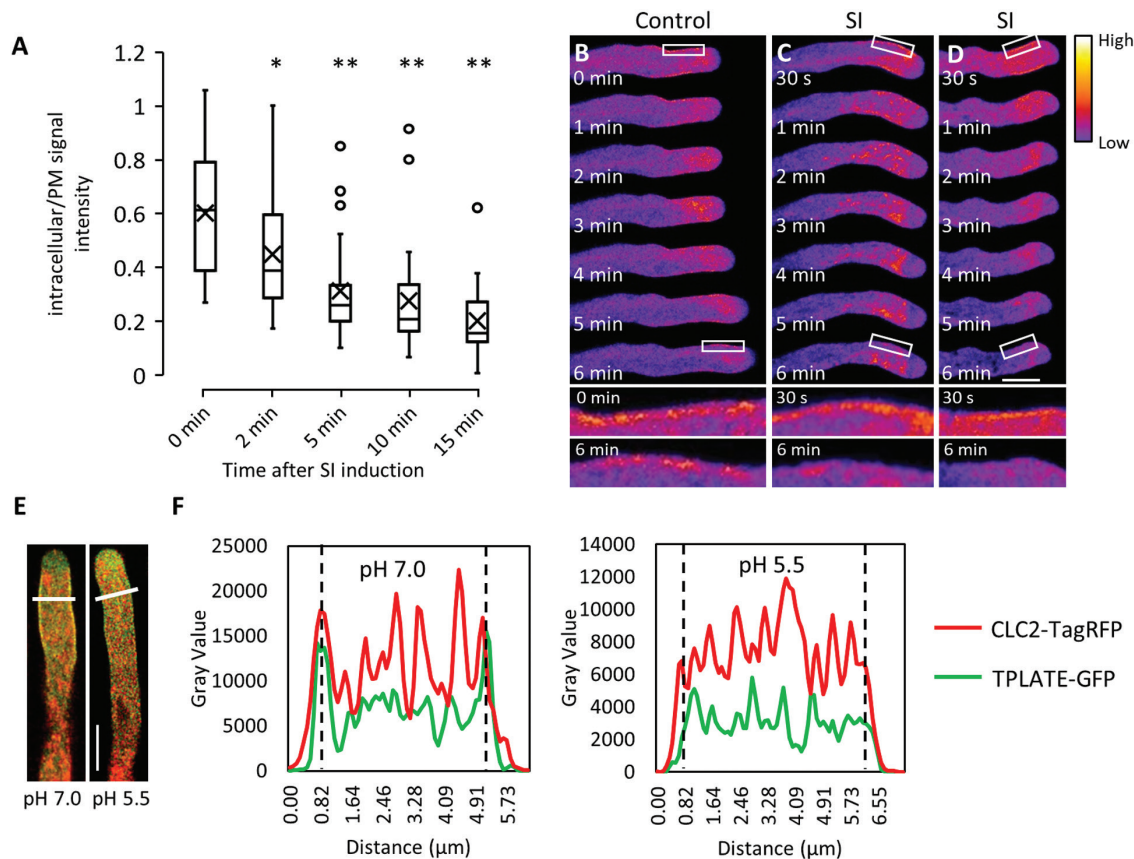


**Fig. 2.** CME is inhibited after SI induction and cytosolic acidification. (A) Boxplots showing quantification of the FM4-64 signal intensity as a ratio (in the cytoplasm versus on the plasma membrane) at different time points after SI induction. Significance levels are based on comparisons with '0 min'. \* $P < 0.01$  and \*\* $P < 0.001$  with Kruskal-Wallis ANOVA on ranks ( $n = 34, 31, 30, 28$ , and  $27$  for time points 0, 2, 5, 10, and 15 min, respectively). (B) Time-lapse fluorescent images showing the localization of TPLATE-TagRFP at the subapical plasma membrane region of a growing pollen tube; see also higher magnification images of selected areas (white box) after 0 min and 6 min. (C and D) After SI induction, the localization of TPLATE-TagRFP at the plasma membrane is rapidly lost; see also higher magnification images after 6 min. The position of the RFP signal on the plasma membrane immediately after treatment is clearly visible at higher magnification. The fluorescence intensity of TPLATE-TagRFP is indicated by the colour gradient. Corresponding fluorescence intensity profiles are shown in Supplementary Fig. S2. Scale bar = 10  $\mu\text{m}$ . (E) Representative images showing the co-localization of TPLATE-GFP (green) and CLC2-TagRFP (red) at the plasma membrane at cytosolic pH 7.0 while plasma membrane recruitment is abolished at pH 5.5. Scale bar = 10  $\mu\text{m}$ . (F) Fluorescence intensity profiles for the pollen tubes along the white lines indicated in (E). Dashed lines indicate the position of the plasma membrane.

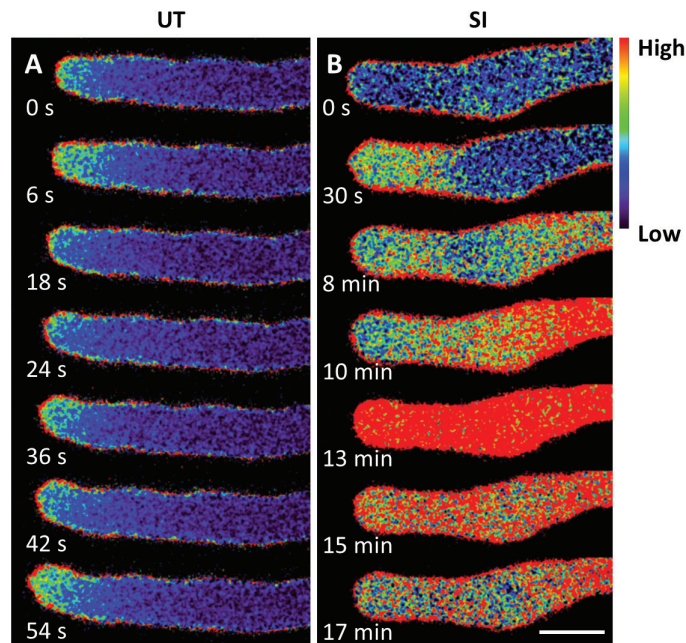


**Fig. 3.** Cytosolic free  $\text{Ca}^{2+}$  increases in Arabidopsis pollen tubes during the SI response. Representative ratio-imaging examples of Arabidopsis pollen tubes expressing *PrpS<sub>1</sub>* and YC3.6 without treatment (A, untreated, UT) and after treatment with *PrsS<sub>1</sub>* (B, SI). Scale bar = 10  $\mu\text{m}$ .

tubes during the SI response, we used the genetically encoded fluorescent  $\text{Ca}^{2+}$  sensor YC3.6 (Nagai *et al.*, 2004) to monitor alterations in  $[\text{Ca}^{2+}]_{\text{cyt}}$ . Ratio-imaging of untreated growing pollen tubes co-expressing *PrpS<sub>1</sub>* and YC3.6 revealed a tip-focused  $[\text{Ca}^{2+}]_{\text{cyt}}$  gradient associated with tip growth (Fig. 3A), previously observed in many pollen tubes growing *in vitro*, including *Papaver* and Arabidopsis pollen tubes (Franklin-Tong *et al.*, 1997; Hepler *et al.*, 2001; Iwano *et al.*, 2009). After addition of *PrsS<sub>1</sub>* to induce the SI response, ratio-imaging revealed that the apical  $[\text{Ca}^{2+}]_{\text{cyt}}$  gradient rapidly dissipated (within 1 min), and a more dispersed area of elevated  $[\text{Ca}^{2+}]_{\text{cyt}}$  was observed in the general tip region (Fig. 3B). This area of elevated  $[\text{Ca}^{2+}]_{\text{cyt}}$  extended further back into the shank area at 8 min. Ten minutes after SI induction, a dramatic increase of  $[\text{Ca}^{2+}]_{\text{cyt}}$  was detected in the shank area and appeared to peak at 13 min (Fig. 3B). Subsequently, the  $[\text{Ca}^{2+}]_{\text{cyt}}$  decreased. These results are similar to the SI-induced spatio-temporal changes for  $[\text{Ca}^{2+}]_{\text{cyt}}$  reported in *Papaver* pollen tubes (Franklin-Tong *et al.*, 1997). This demonstrates that the genetically encoded marker YC3.6 allows us to monitor and describe the  $[\text{Ca}^{2+}]_{\text{cyt}}$  signature during the SI response.

#### *PrsS–PrpS interaction triggers actin remodelling*

Dramatic SI-induced remodelling of the F-actin cytoskeleton has been described in both incompatible *Papaver* pollen tubes (Geitmann *et al.*, 2000; Snowman *et al.*, 2002; Poulter *et al.*, 2010) and transgenic Arabidopsis pollen tubes expressing *PrpS* (de Graaf *et al.*, 2012). However, previous data used fixed pollen tubes from a few time points and relied on the staining of F-actin with phalloidin. Here we used the genetically encoded filamentous actin probe Lifeact-mRuby2 (Riedl *et al.*,

2008; Bascom *et al.*, 2018) to initiate investigations into the dynamic remodelling of the actin cytoskeleton in incompatible pollen tubes using live-cell imaging. In an untreated pollen tube, the F-actin arrays comprise filament bundles that are arranged longitudinally and parallel to the growth axis, and pollen tube growth is evident (Fig. 4A). After SI induction, the F-actin cytoskeleton rapidly altered and formation of punctate F-actin foci, a signature event of the SI response, was observed (Fig. 4B–D; Supplementary Movie S2).

Different Arabidopsis lines expressing *PrpS<sub>1</sub>* with Lifeact-mRuby2 together with other markers varied in their response times. Pollen tubes with high expression levels of *PrpS<sub>1</sub>* exhibited a more rapid response compared with lines with much lower expression levels of *PrpS<sub>1</sub>* (Fig. 1C; Supplementary Table S1); we named these ‘rapid’ and ‘slow’ lines, respectively. In a ‘rapid’ transgenic Arabidopsis line, incompatible pollen tubes co-expressing *PrpS<sub>1</sub>* and Lifeact-mRuby2 exhibited a rapid SI response, and F-actin foci were usually observed within 10 min after SI induction (Fig. 4B; Supplementary Movie S2). Within a few minutes of SI induction in a representative ‘rapid’ pollen tube, the longitudinal F-actin bundles disappeared, while predominant cortical F-actin bundles adjacent to the plasma membrane remained. From ~4–5 min onwards, F-actin foci started to form (Fig. 4B). This rapidly reacting line enabled us to observe the entire process of actin remodelling during SI, allowing observation of the progression of actin filaments into foci structures (Supplementary Movie S2), which could not be achieved with conventional fixation approaches.

To further dissect the actin dynamics in incompatible pollen tubes, a ‘slow’ transgenic Arabidopsis line was utilized to obtain spatio-temporal details of the F-actin reorganization (Fig. 4C–D, F–G). Mid-plane images of a representative pollen tube (Fig. 4C) revealed that even 15 min after SI induction, small numbers of thick actin filament bundles were still apparent; these disappeared ~30 min after SI induction. Actin filaments in the cortical region appeared to become shorter and dramatically reorganized, forming a ‘fishing net’ pattern, suggesting that they were severed (Fig. 4D). By 60 min, the actin population in this cortical region fragmented further, appearing to form small foci. Later, these F-actin foci increased in size.

To characterize the F-actin remodelling during SI further, we used kymograph analysis to monitor the SI-induced changes in dynamics of F-actin at the cortex of pollen tubes from a ‘rapid’ line (Fig. 4E; Supplementary Movie S2). This shows two distinct areas: one area apparent during early SI, with a rather random signal that shows highly dynamic F-actin adjacent to the plasma membrane; and another area later (after 6–7 min), appearing as multiple straight lines. This latter observation shows that the punctate actin foci are not dynamic and do not move (Fig. 4E). As the transition between these two areas is quite distinct, it shows that the change from dynamic F-actin filament arrays to highly stable F-actin foci is rapid. This reveals that (at least at the cortical region of these rapidly responding pollen tubes), the formation of foci is a sudden event rather than a gradual development. Further analyses will be needed to determine if formation of foci in the centre of pollen tubes is similar to that in the cortical region.



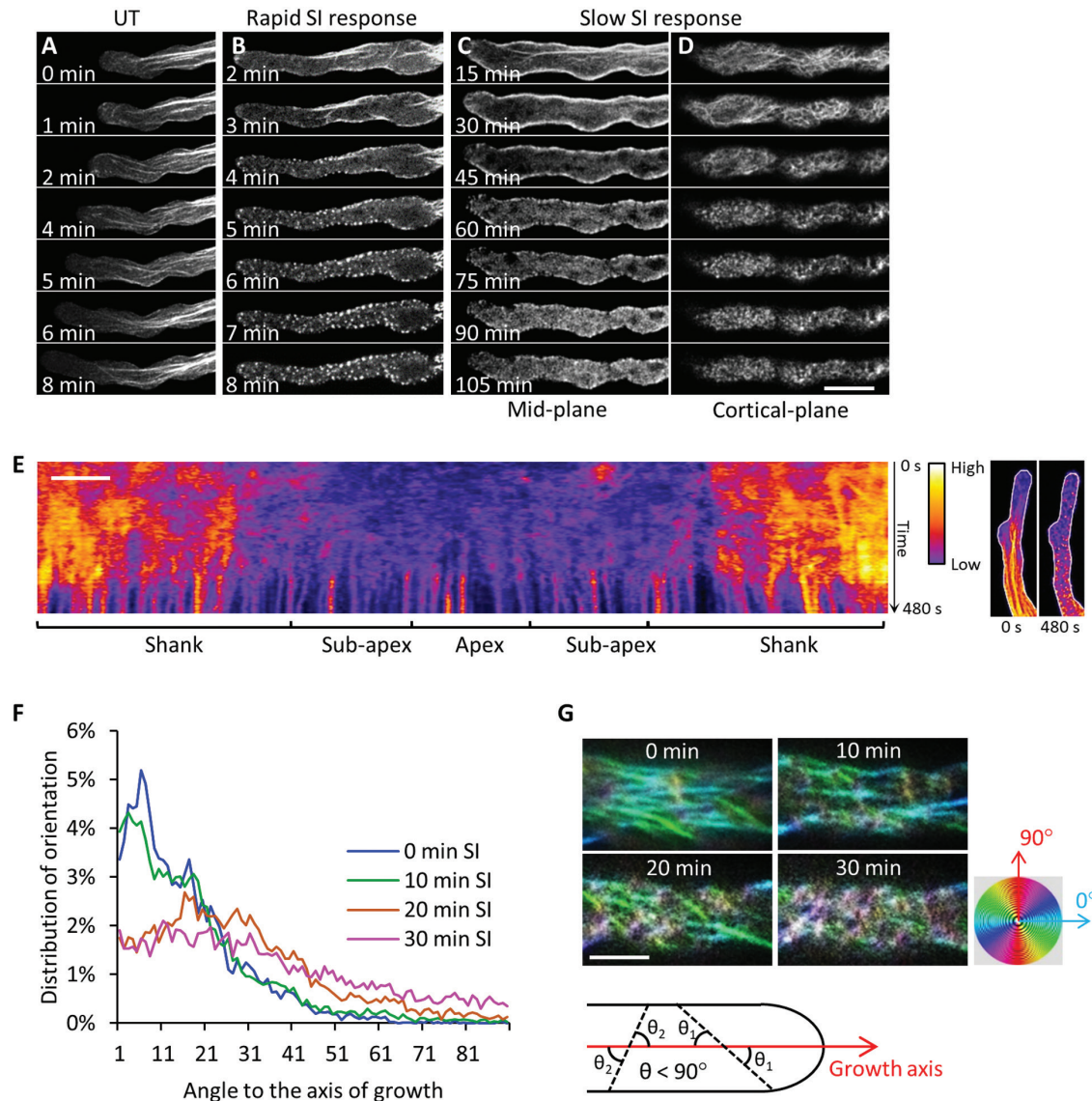


**Fig. 4.** F-actin remodelling in Arabidopsis pollen tubes during the SI response. (A–D) Time-lapse images showing SI-induced remodelling of the F-actin cytoskeleton using Lifeact-mRuby2 as a marker, in pollen tubes of two Arabidopsis lines with different expression levels of *PrpS<sub>1</sub>*. (A) The F-actin cytoskeleton of an untreated growing pollen tube. (B) Remodelling of the F-actin cytoskeleton during an SI response in an Arabidopsis ‘rapid’ line with a high level of expression of *PrpS<sub>1</sub>*. (C) Mid-plane images of a time-lapse sequence showing remodelling of the F-actin cytoskeleton during an SI response in an Arabidopsis ‘slow’ line with a low level of expression of *PrpS<sub>1</sub>*. (D) Cortical plane images of the pollen tube shown in (C). (E) Pseudocoloured kymograph analysis of F-actin (monitored with Lifeact-mRuby2) adjacent to the plasma membrane of a representative pollen tube (maximum projection) during the SI response in a ‘rapid’ line. The fluorescence intensity in the kymograph indicates the amount of F-actin near the plasma membrane of the pollen tube (shown by white lines in the images on the right). The fluorescence intensity is indicated by the colour gradient. Scale bar=5  $\mu\text{m}$ . (F) Alterations in the distribution of the angles between F-actin filaments and the growth axis of the pollen tube at different time points after SI induction. (G) Representative images show the rearrangement of F-actin filament arrays at the cortical region of pollen tubes during the early stages of SI. The spectrum disc indicates the pseudocolours applied to actin filaments based on their orientations relative to the growth axis of the pollen tube. The diagram demonstrates the angles ( $\theta_1$ ,  $\theta_2$  ...) between actin filaments (dashed lines) and the growth axis (red arrow) of the pollen tube. Only the sharp angles ( $\theta < 90^\circ$ ) were measured. Scale bar=10  $\mu\text{m}$ .

To characterize the distinctive patterns formed by F-actin in the cortical region during the early stages of the SI response, we quantified the orientation of actin filaments at different time points during the first 30 min after SI induction in a ‘slow’ line (Fig. 4F). At time 0, the orientation of F-actin bundles was mostly parallel to the growth axis, predominantly distributed between  $0^\circ$  and  $30^\circ$  relative to the growth axis (Fig. 4F). Imaging at 10 min after SI induction showed that a small proportion of actin bundles had reorientated relative to the growth axis (Fig. 4G). After 20 min, the F-actin bundles reorientated further to form the ‘fishing net’ pattern (Fig. 4G),

reflected by the wider distribution of angles (Fig. 4F). After 30 min, F-actin bundles appeared to be randomly orientated relative to the growth axis (Fig. 4G) with angles distributed throughout  $0$ – $90^\circ$  (Fig. 4F). These observations begin to describe the actin remodelling during the SI response.

#### *PrpS–PrsS interaction triggers decreases in cytosolic pH*

The PrpS–PrsS interaction triggers dramatic intracellular acidification which acts as an important regulatory factor of the SI

response in *Papaver* (Bosch and Franklin-Tong, 2007; Wilkins et al., 2015; Wang et al., 2019). To further investigate the regulatory role of cytosolic acidification in *Papaver* SI-PCD, we made a transgenic Arabidopsis ‘SI’ line co-expressing Lifeact-mRuby2 and a pH indicator, pHGFP (Moseyko and Feldman, 2001). This ‘rapid’ line (Fig. 4E) enabled us to capture SI-induced changes in  $[pH]_{\text{cyt}}$  and remodelling of F-actin in the same pollen tube (Fig. 5A, B). Two minutes after SI induction, the  $[pH]_{\text{cyt}}$  rapidly decreased, while thick F-actin bundles in the central region of the pollen tube remained. Four minutes after SI induction, the  $[pH]_{\text{cyt}}$  further dropped to a mean value of approximately pH 6.0 (Fig. 5A), and small F-actin foci started to be visible in the region close to the tip (Fig. 5B). By 7 min, the mean  $[pH]_{\text{cyt}}$  had decreased further (Fig. 5A) and large F-actin foci had formed and were distributed throughout the pollen tube (Fig. 5B). The extent of SI-induced cytosolic acidification, determined using this genetically encoded pH indicator (Fig. 5C), was similar to that previously reported for incompatible *Papaver* pollen tubes (Wilkins et al., 2015), although the  $[pH]_{\text{cyt}}$  decreased faster (Fig. 1C), probably due to the high expression level of PrpS<sub>1</sub>. The ability to monitor  $[pH]_{\text{cyt}}$  and F-actin within the same pollen tube provides a valuable tool to investigate mechanistic links between cytosolic pH and dynamic remodelling of the actin cytoskeleton during the SI response in the future.

#### *PrpS–PrsS interaction triggers co-localization of CAP1 and ADF7 with F-actin foci*

In *Papaver*, two ABPs, CAP and ADF, co-localized with F-actin foci after SI induction and after artificially lowering the  $[pH]_{\text{cyt}}$

to 5.5 (Poulter et al., 2010; Wilkins et al., 2015). This suggested that they may play important roles in the formation of foci. We generated ‘SI’ Arabidopsis lines co-expressing fluorescently tagged Arabidopsis CAP1 and ADF7: CAP1–mTagBFP2 or ADF7–mTagBFP2 with Lifeact–mRuby2, which enabled us to simultaneously detect the respective ABP and F-actin (Fig. 6). In untreated pollen tubes, ADF7–mTagBFP2 was distributed homogeneously throughout the pollen tube cytosol (Fig. 6B). CAP1–mTagBFP2 showed a similar distribution, however with a slightly more speckled appearance. Two hours after SI induction, both ABPs had formed structures that resemble F-actin foci (Fig. 6D, E, J, K), and both ABPs co-localized with the F-actin foci (Fig. 6F, L). These live-cell observations correspond to previous findings in fixed and stained *Papaver* pollen tubes (Poulter et al., 2010), providing good evidence that transgenic Arabidopsis ‘SI’ pollen tubes undergo a similar SI response. This suggests that these ABPs are likely to play mechanistic roles in mediating actin dynamics and foci formation during SI. Thus, this new approach of dual labelling of ABPs and F-actin with live-cell imaging provides us with powerful tools to help establish the functional roles of CAP1 and ADF7 in SI-PCD in the future.

#### *PrpS–PrsS interaction triggers alterations in vacuolar morphology*

Previous studies revealed reorganization of the vacuole in *Papaver* pollen tubes after SI induction (Wilkins et al., 2015; Wang et al., 2019). Here we used Arabidopsis ‘SI’ pollen expressing VAMP711–mCherry (WAVE9R; Geldner et al., 2009), which localizes to the vacuolar membrane, to monitor changes

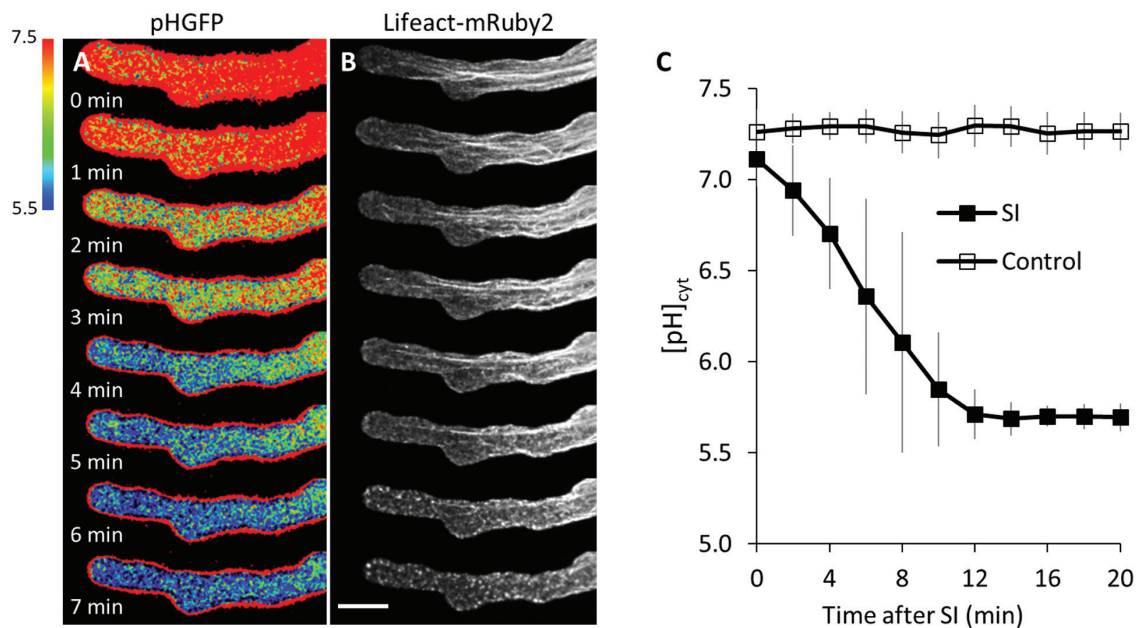


**Fig. 5.** Rapid cytosolic acidification and remodelling of the actin cytoskeleton in Arabidopsis pollen tubes during the SI response. (A) Representative time-lapse ratio-images of pHGFP in pollen tubes of a ‘rapid’ line after treatment with PrpS<sub>1</sub> to induce SI. (B) Remodelling of F-actin visualized with Lifeact-mRuby2 in the same pollen tube as shown in (A) during the SI response. Scale bar=10  $\mu$ m. (C) Quantification of the changes in cytosolic pH after SI induction (SI;  $n=20$ ) or treatment with inactivated PrpS<sub>1</sub> (control;  $n=10$ ). Error bars indicate the SD.



in vacuolar morphology during SI. In untreated growing pollen tubes, a reticulate structure was observed throughout the pollen tube shank; this arrangement has been described in growing *Arabidopsis* pollen tubes by Hicks *et al.* (2004). The different vacuolar organizations observed after SI induction in the heterologous *Arabidopsis* 'SI' system were classified into different morphologies (Fig. 7A, B). We identified a series of changes to the vacuolar appearance ('morphology B–G', Fig. 7A), with different sized globular structures formed over time. Quantification of these morphological changes showed evidence of a distinct progression over time (Fig. 7B). These data show that the genetically encoded vacuolar marker WAVE9R allows visualization of SI-induced changes to the organization of pollen tube vacuoles.

#### *PrpS–PrsS interaction triggers a DEVDase/caspase-3-like activity and cell death*

Proteases exhibiting caspase-like activities have been implicated in many PCD-related events in plants (Sueldo and van der Hoorn, 2017). Previous studies showed that SI-induced PCD in *Papaver* involves a DEVDase/caspase-3-like activity (Thomas and Franklin-Tong, 2004; Bosch and Franklin-Tong, 2007) and that pre-treatment of pollen expressing *Papaver* PrpS with the caspase-3 inhibitor Ac-DEVD-CHO reduced S-specific death (Thomas and Franklin-Tong, 2004; Bosch and Franklin-Tong, 2008; de Graaf *et al.*, 2012). Here we used the fluorescent probe Ac-DEVD-AMC to more directly determine if a cognate PrpS–PrsS interaction triggers a DEVDase/caspase-3-like activity in *Arabidopsis* lines expressing PrpS<sub>1</sub>. Caspase-3 cleaves the tetrapeptide, releasing the fluorogenic AMC, which can be imaged to assess DEVDase activity in pollen grains. After SI, an increase in fluorescence, indicating an increase in DEVDase activity, was observed (Fig. 8A, B).

This increase in activity was significantly reduced when pollen was pre-treated with the caspase-3 inhibitor Ac-DEVD-CHO (Fig. 8A). The increase in caspase-3-like activity was significantly different compared with those pre-treated with the inhibitor from 4 h after SI induction ( $***P < 0.001$ , Wilcoxon, Fig. 8A). We also used the genetically encoded fluorescently-tagged NLS–tdTomato to follow nuclear integrity and disruption in SI-induced pollen, as nuclear permeabilization is typical for apoptosis in animal cells (Taylor *et al.*, 2008). An increasing number of pollen grains lost their fluorescence signal of NLS–tdTomato in the nucleus after SI induction, indicating disruption of nuclei (Fig. 8C). Together, these data confirm that a cognate PrpS–PrsS interaction leads to a similar endpoint to *Papaver* SI-PCD in the engineered *Arabidopsis* 'SI' system, with cell death utilizing a DEVDase/caspase-3-like activity.

## Discussion

Pollination events are complex, crucial steps in plant reproduction leading to fertilization and seed set. This not only provides an intriguing system to study fundamental processes involved in tip growth (a topic of this Special Issue), but we also anticipate that a better mechanistic understanding may eventually provide tools that can be used in improving crop production. By studying cellular alterations that can stop tip growth, one can achieve insights into events controlling growth. SI in *Papaver rhoeas* triggers a signalling network resulting in inhibition of pollen tube tip growth and subsequent PCD of incompatible pollen. The development of an *in vitro* bioassay to study *Papaver* SI using S-specific inhibition of pollen tube growth has played a key part in advancing our mechanistic understanding of how this is achieved and has positioned the *Papaver* SI system as one of the best understood SI systems in the plant kingdom. Moreover, by uncovering a complex and elaborate network of

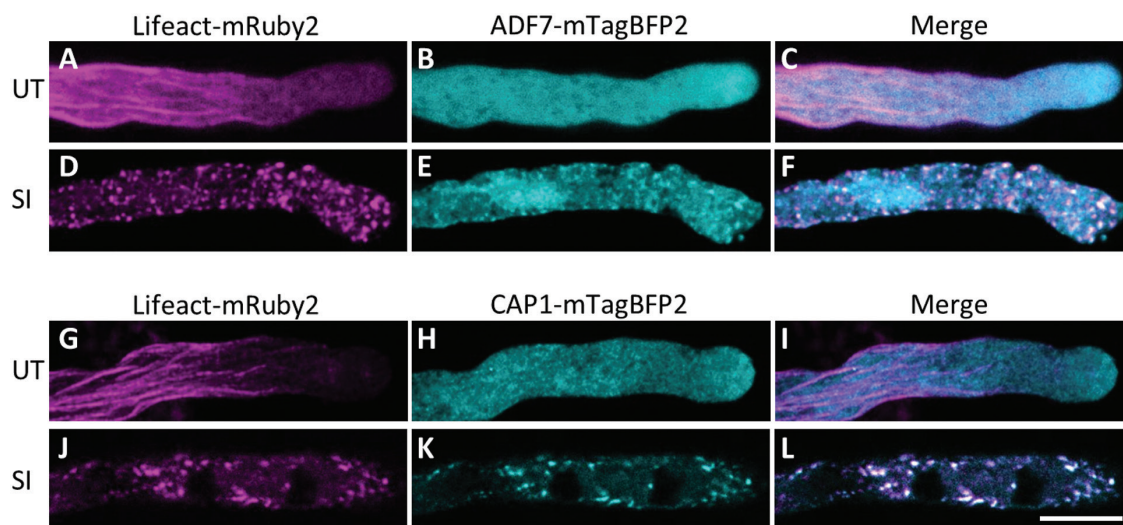


**Fig. 6.** SI induction leads to the co-localization of ADF7 and CAP1 with F-actin foci. ADF7–mTagBFP2, CAP1–mTagBFP2 (both in cyan), and F-actin localization (Lifeact–mRuby2 in magenta) are shown in untreated pollen tubes expressing *PrpS*<sub>1</sub> (A–C and G–I) or after SI induction (D–F and J–L). In untreated pollen tubes, ADF7 and CAP1 were distributed throughout the cytoplasm, with no major co-localization with F-actin (C and I). After SI induction, ADF7 and CAP1 co-localized with F-actin foci (F and L, respectively). Co-localization shows as white. Scale bar = 10 μm.

events involved in inhibition, these studies have contributed to our understanding of how tip growth is regulated.

Although the *Papaver* SI system has provided an excellent model system to investigate cell–cell recognition, intracellular signalling, and PCD at a molecular level, the extremely limited genetic resources in this system represent a serious bottleneck. The development of transgenic Arabidopsis lines with functional *PrpS* expressed in its pollen (De Graaf et al., 2012) and later functional transfer of both *Papaver* SI S-determinants to Arabidopsis reproduction *in planta* (Lin et al., 2015) demonstrated that the two components, PrpS and PrsS, are sufficient to elicit an SI response in another species. This successful functional transfer suggests that the components involved in the SI events of *Papaver*, downstream of the cognate interaction of the S-determinants that triggers the SI response, may be conserved in pollen tubes and are likely to be ancient, as they could be successfully recruited in a distantly related species (Lin et al., 2015). The availability of Arabidopsis plants expressing an SI response with all the key features of *Papaver* SI opens up exciting new opportunities to genetically dissect SI-induced signalling networks.

Here we have described the first use of fluorescent genetic tools such as YC3.6 to follow SI-induced alterations in  $[Ca^{2+}]_{\text{cyt}}$ , pHGFP to monitor  $[pH]_{\text{cyt}}$ , LifeAct-mRuby2 to follow remodelling of the actin cytoskeleton, mCherry expressed at the tonoplast to visualize alterations in vacuolar morphology, and NLS–tdTomato to observe nuclear disruption. We have shown that this heterologous system is robust and allows us to perform detailed live-cell imaging of key events involved in *Papaver* SI. These results highlight the

opportunities for using genetically encoded markers/probes to deepen our understanding of this important SI system. A particular strength of this transgenic system is that it facilitates investigating links between different cellular events (e.g. pH and actin dynamics) by multiparameter imaging and identifying new components involved in/affected by SI induction. Moreover, we can manipulate the speed of the response to suit what we wish to investigate by using lines with higher or lower PrpS expression levels. For instance, the use of ‘rapid’ (high expressing) lines enabled us to image and analyse the entire process of the SI-induced reorganization of the F-actin cytoskeleton, from highly dynamic long filament bundles to stable foci. Use of ‘slow’ (low expressing) lines, which more closely resemble the timing of SI-induced events reported for *Papaver* (Bosch and Franklin-Tong, 2008; Wilkins et al., 2014; Wang et al., 2019), facilitates capturing transient events that occur early during SI, for instance CME (discussed below), and the detailed dissection of changes in actin dynamics during the SI response.

In addition to providing higher temporal resolution of SI-induced events than were previously described in *Papaver*, genetically encoded probes can also identify new events involved. Here we provide the first evidence that CME is rapidly inhibited during SI. TPLATE interacts with clathrin (Van Damme et al., 2011) and is part of a unique multisubunit protein complex (TPLATE complex, TPC), which is connected to the early events of CME at the plasma membrane in concert with the adaptor protein complex 2 (AP-2) (Van Damme et al., 2011; Gadeyne et al., 2014). The dislodging of TPLATE from the plasma membrane and the inhibition of FM4-64

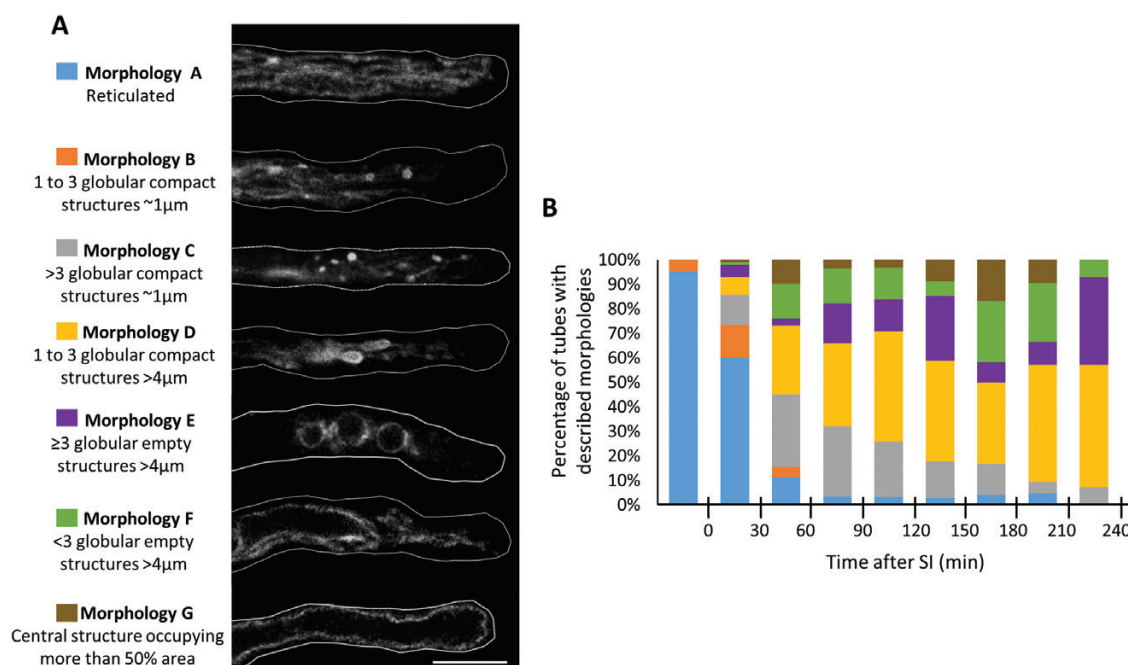


**Fig. 7.** Changes in vacuolar morphologies in pollen tubes during the SI response. (A) Categorization and descriptions of different vacuolar morphologies observed in transgenic Arabidopsis pollen tubes after SI induction. The different morphologies were categorized according to the distribution of VAMP711–mCherry, a vacuolar membrane-localized protein, in the median focal plane of the pollen tubes. Scale bar=10 µm. (B) Quantification of pollen tubes exhibiting the vacuolar morphologies shown in (A) at different time points during the SI response.

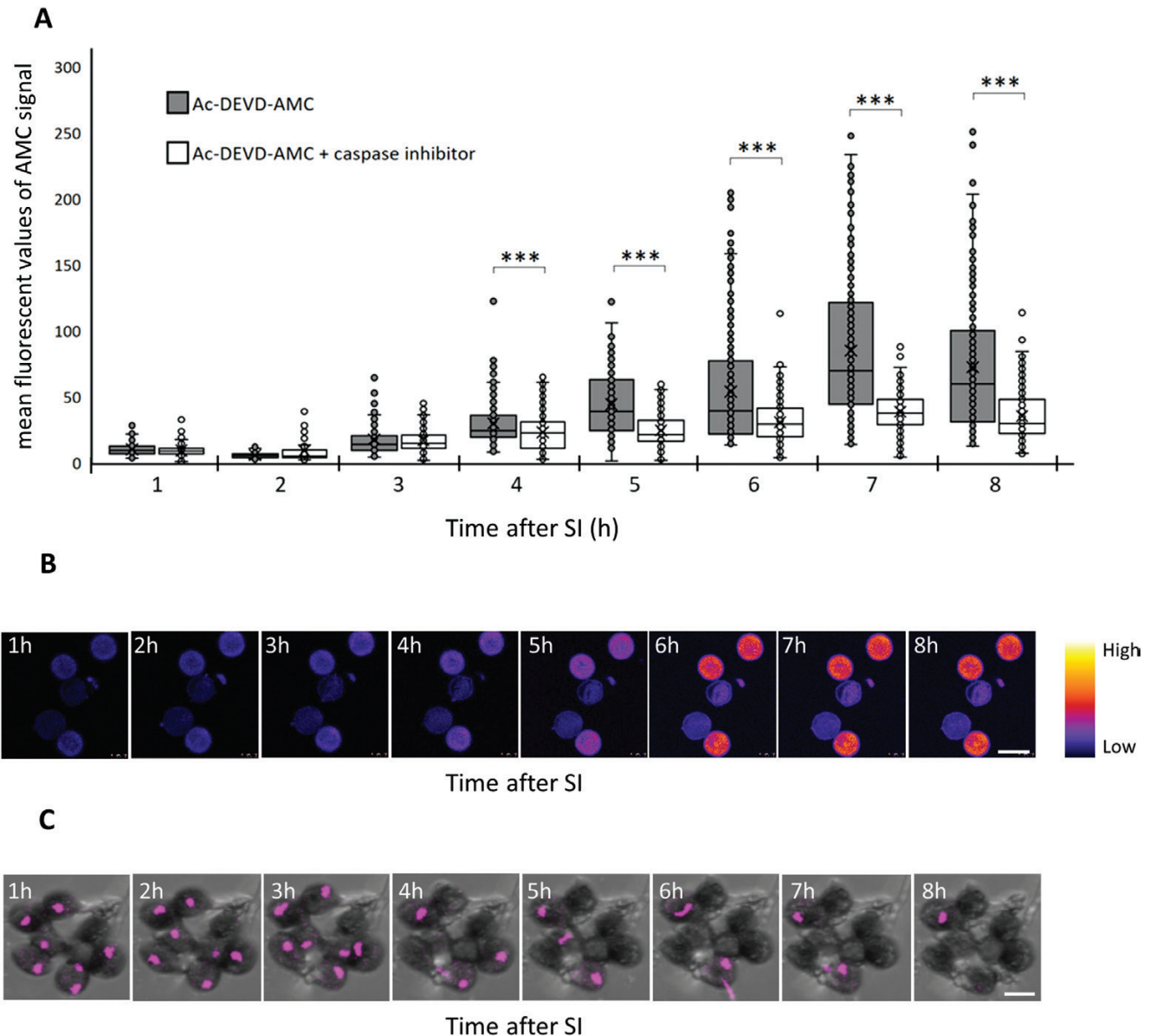


**Fig. 8.** SI induction activates a DEVDase/caspase-3-like activity and nuclear disruption in Arabidopsis pollen. (A) Quantification of AMC fluorescence provides a measure of DEVDase/caspase-3-like activity in pollen grains during the SI response in the absence/presence of the caspase-3 inhibitor Ac-DEVD-CHO ( $n=100-350$ ). (B) Representative time-lapse images showing the increase in the AMC fluorescent signal in pollen grains after SI induction. Scale bar=20  $\mu\text{m}$ . (C) Nuclear disruption after SI induction indicated by the loss of NLS-tdTomato signal (magenta) in the nucleus. Scale bar=20  $\mu\text{m}$ .

internalization soon after SI induction (Fig. 2A–D) provide strong evidence that the CME machinery is disrupted early on (within the first few minutes) during the SI response. The dissipation of TPLATE and CLC2 from the plasma membrane after treatment with propionic acid at low pH (pH 5.5) is in agreement with earlier work on Arabidopsis root cells where CME was inhibited by cytoplasmic acidification (Dejonghe *et al.*, 2016). Moreover, caffeine addition to dividing tobacco BY-2 cells has been shown to dislodge TPLATE and clathrin from the growing cell plate within minutes after caffeine addition (Van Damme *et al.*, 2011). Caffeine is linked to the modulation of  $[\text{Ca}^{2+}]_{\text{cyt}}$ , and  $[\text{Ca}^{2+}]_{\text{cyt}}$  has been shown to inhibit phospholipid  $[\text{PI}(4,5)\text{P}_2]$  recognition by PH domain-containing proteins (Bilkova *et al.*, 2017). As negatively charged phospholipids are involved in adaptor complex recruitment in animal cells (Kelly

*et al.*, 2014), the dislodgement of the endocytic machinery from the plasma membrane of the pollen tubes might therefore be caused by a combined action of acidification as well as SI-induced increases in  $[\text{Ca}^{2+}]_{\text{cyt}}$ , which occur prior to the inhibition of pollen tube growth (Franklin-Tong *et al.*, 1993, 1997). Together with the rise in  $[\text{Ca}^{2+}]_{\text{cyt}}$  and the depolymerization/reorganization of the actin cytoskeleton, the disruption of CME represents another very early event that may contribute to, or be a consequence of, the rapid pollen tube growth inhibition after SI. The Arabidopsis ‘SI’ system provides us with the genetic tools to dissect cause and effect regarding CME inhibition and pollen tube growth inhibition, and to investigate potential links between CME, pH, and the actin cytoskeleton.

These studies have also revealed, for the first time, details about the early SI-induced dynamic reorganization of



F-actin filament bundles over time. Previously, we only had images of a few fixed time points during SI. Now we have been able to begin to visualize reorganization of filaments into different arrays and fragmentation and shortening of filaments in real time, suggesting that severing may be involved at the earlier stages. Later after SI induction, kymograph analyses revealed that F-actin adjacent to the plasma membrane suddenly alters from being highly dynamic to quite static. The organization and regulation of the actin cytoskeleton have been thoroughly studied in pollen tubes and proven to be crucial for pollen tube growth (reviewed by Qu *et al.*, 2015). A set of ABPs have been found to be important for the spatial distribution and dynamics of the actin cytoskeleton (reviewed by Staiger *et al.*, 2010). Amongst these ABPs, at least two are associated with SI-induced actin foci: ADF7 and CAP1 (Poulter *et al.*, 2010). ADF7 severs actin filaments and promotes normal pollen tube growth by mediating actin filament turnover (Zheng *et al.*, 2013). CAP1 is a major player in regulating actin turnover via its nucleotide exchange activity by synergizing with ADF and profilin (Jiang *et al.*, 2019). Intriguingly, it has been established that the activities of these two ABPs are pH sensitive (Carlier *et al.*, 1997; Gungabissoon *et al.*, 1998; Allwood *et al.*, 2002; Chen *et al.*, 2002; Lovy-Wheeler *et al.*, 2006). The SI-induced drop in  $[pH]_{\text{cyt}}$  may therefore alter the activities of these ABPs, which may contribute to the observed dramatic reorganization of the actin cytoskeleton through alterations of actin dynamic events such as nucleation, severing, bundling/debundling, aggregation, etc. The Arabidopsis 'SI' lines dual-labelling actin and other factors provide us with powerful tools to explore the mechanistic links between the actin cytoskeleton and other regulatory events in *Papaver* SI.

In the future, the availability of transgenic 'SI' Arabidopsis plants with all the key features of the *Papaver* SI system will allow us to overcome the bottleneck of limited genetic resources of *P. rhoeas*. Full forward and reverse genetics toolboxes available for this model plant, such as CRISPR or T-DNA mutant lines, gene silencing/overexpression lines, and lines with fluorescent markers, can now be exploited for further dissecting the molecular mechanisms involved in SI-PCD. These approaches could be employed to identify new factors involved in *Papaver* SI-PCD, especially those that are important to tip growth, as well as the components involved in the later 'execution' phase of the SI-induced PCD process. In summary, using genetically encoded fluorescent probes in combination with live-cell imaging, we were able to confirm and evaluate a range of early events known to be crucial for *Papaver* SI (increase in  $[Ca]_{\text{cyt}}$ , decrease in  $[pH]_{\text{cyt}}$ , and alterations of the actin cytoskeleton), as well as later events (alterations of vacuolar morphologies and PCD). In addition, we identified CME inhibition as a new event affected early on by SI. As such, this study has provided further evidence of the suitability and opportunities that the heterologous Arabidopsis 'SI' system provides to further our understanding of SI-PCD in *Papaver* and for testing new hypotheses about the cellular mechanisms and genetic components involved in the SI-PCD response and tip growth of plant cells.

## Supplementary data

Supplementary data are available at JXB online.

Movie S1. Growth arrest of an Arabidopsis pollen tube after SI induction.

Movie S2. F-actin reorganization and foci formation during the SI response.

Supplementary Protocols. Construction of transgenic Arabidopsis lines.

Fig. S1. Diagram of the transgene cassettes that were used for transformation of *Arabidopsis thaliana* in this study.

Fig. S2. TPLATE-TagRFP localizes at the plasma membrane.

Table S1. Overview of transgenic Arabidopsis lines used in this study.

Table S2. Oligonucleotides used for transgene construction and expression analysis.

## Acknowledgements

We gratefully acknowledge funding by the Biotechnology and Biological Sciences Research Council (grant no. BB/P005489/1) to VEF-T and MB, the European Research Council (ERC) Starting Grant PROCELLDEATH (project no. 749 639234) to MKN, and funding by the Fonds Wetenschappelijk Onderzoek - Vlaanderen (FWO) (project nos G011215N and 12I7417N) to MT and ZL, respectively. We thank Magdalena Bezanilla (Dartmouth College) for providing Lifeact-mRuby2.

## References

- Allwood EG, Anthony RG, Smertenko AP, Reichelt S, Drobak BK, Doonan JH, Weeds AG, Hussey PJ. 2002. Regulation of the pollen-specific actin-depolymerizing factor LIADF1. *The Plant Cell* **14**, 2915–2927.
- Barnanas B, Fridvalsky L. 1984. Adhesion and germination of differently treated maize pollen grains on the stigma. *Acta Botanica Hungarica* **30**, 329–332.
- Bascom CS Jr, Winship LJ, Bezanilla M. 2018. Simultaneous imaging and functional studies reveal a tight correlation between calcium and actin networks. *Proceedings of the National Academy of Sciences, USA* **115**, E2869–E2878.
- Bedinger PA, Broz AK, Tovar-Mendez A, McClure B. 2017. Pollen–pistil interactions and their role in mate selection. *Plant Physiology* **173**, 79–90.
- Bilkova E, Pleskot R, Rissanen S, *et al.* 2017. Calcium directly regulates phosphatidylinositol 4,5-bisphosphate headgroup conformation and recognition. *Journal of the American Chemical Society* **139**, 4019–4024.
- Bosch M, Franklin-Tong VE. 2007. Temporal and spatial activation of caspase-like enzymes induced by self-incompatibility in *Papaver* pollen. *Proceedings of the National Academy of Sciences, USA* **104**, 18327–18332.
- Bosch M, Franklin-Tong VE. 2008. Self-incompatibility in *Papaver*: signalling to trigger PCD in incompatible pollen. *Journal of Experimental Botany* **59**, 481–490.
- Carlier MF, Laurent V, Santolini J, Melki R, Didry D, Xia GX, Hong Y, Chua NH, Pantaloni D. 1997. Actin depolymerizing factor (ADF/cofilin) enhances the rate of filament turnover: implication in actin-based motility. *Journal of Cell Biology* **136**, 1307–1322.
- Chen CY, Wong EI, Vidali L, Estavillo A, Hepler PK, Wu HM, Cheung AY. 2002. The regulation of actin organization by actin-depolymerizing factor in elongating pollen tubes. *The Plant Cell* **14**, 2175–2190.
- de Graaf BH, Vátovec S, Juárez-Díaz JA, Chai L, Kooblall K, Wilkins KA, Zou H, Forbes T, Franklin FC, Franklin-Tong VE. 2012. The *Papaver* self-incompatibility pollen S-determinant, PrpS, functions in *Arabidopsis thaliana*. *Current Biology* **22**, 154–159.
- Dejonghe W, Kuenen S, Mylle E, *et al.* 2016. Mitochondrial uncouplers inhibit clathrin-mediated endocytosis largely through cytoplasmic acidification. *Nature Communications* **7**, 11710.

- Dresselhaus T, Franklin-Tong N.** 2013. Male–female crosstalk during pollen germination, tube growth and guidance, and double fertilization. *Molecular Plant* **6**, 1018–1036.
- Franklin-Tong VE, Gourelay CW.** 2008. A role for actin in regulating apoptosis/programmed cell death: evidence spanning yeast, plants and animals. *The Biochemical Journal* **413**, 389–404.
- Franklin-Tong VE, Hackett G, Hepler PK.** 1997. Ratio-imaging of  $\text{Ca}^{2+}$  in the self-incompatibility response in pollen tubes of *Papaver rhoeas*. *The Plant Journal* **12**, 1375–1386.
- Franklin-Tong VE, Ride JP, Franklin FCH.** 1995. Recombinant stigmatic self-incompatibility (S-) protein elicits a  $\text{Ca}^{2+}$  transient in pollen of *Papaver rhoeas*. *The Plant Journal* **8**, 299–307.
- Franklin-Tong VE, Ride JP, Read ND, Trewavas AJ, Franklin FCH.** 1993. The self-incompatibility response in *Papaver rhoeas* is mediated by cytosolic free calcium. *The Plant Journal* **4**, 163–177.
- Fujii S, Kubo K, Takayama S.** 2016. Non-self- and self-recognition models in plant self-incompatibility. *Nature Plants* **2**, 16130.
- Gadeyne A, Sánchez-Rodríguez C, Vanneste S, et al.** 2014. The TPLATE adaptor complex drives clathrin-mediated endocytosis in plants. *Cell* **156**, 691–704.
- Geitmann A, Snowman BN, Emons AM, Franklin-Tong VE.** 2000. Alterations in the actin cytoskeleton of pollen tubes are induced by the self-incompatibility reaction in *Papaver rhoeas*. *The Plant Cell* **12**, 1239–1251.
- Geldner N, Dénervaud-Tendon V, Hyman DL, Mayer U, Stierhof YD, Chory J.** 2009. Rapid, combinatorial analysis of membrane compartments in intact plants with a multicolor marker set. *The Plant Journal* **59**, 169–178.
- Grebnev G, Ntefidou M, Kost B.** 2017. Secretion and endocytosis in pollen tubes: models of tip growth in the spot light. *Frontiers in Plant Science* **8**, 154.
- Gungabissoon RA, Jiang CJ, Drobak BK, Maciver SK, Hussey PJ.** 1998. Interaction of maize actin-depolymerising factor with actin and phosphoinositides and its inhibition of plant phospholipase C. *The Plant Journal* **16**, 689–696.
- Hepler PK, Vidali L, Cheung AY.** 2001. Polarized cell growth in higher plants. *Annual Review of Cell and Developmental Biology* **17**, 159–187.
- Hicks GR, Rojo E, Hong S, Carter DG, Raikhel NV.** 2004. Germinating pollen has tubular vacuoles, displays highly dynamic vacuole biogenesis, and requires VACUOLESS1 for proper function. *Plant Physiology* **134**, 1227–1239.
- Iwano M, Entani T, Shiba H, et al.** 2009. Fine-tuning of the cytoplasmic  $\text{Ca}^{2+}$  concentration is essential for pollen tube growth. *Plant Physiology* **150**, 1322–1334.
- Jiang Y, Chang M, Lan Y, Huang S.** 2019. Mechanism of CAP1-mediated apical actin polymerization in pollen tubes. *Proceedings of the National Academy of Sciences, USA* **116**, 12084–12093.
- Kelly BT, Graham SC, Liska N, Dannhauser PN, Höning S, Ungewickell EJ, Owen DJ.** 2014. Clathrin adaptors. AP2 controls clathrin polymerization with a membrane-activated switch. *Science* **345**, 459–463.
- Lin Z, Eaves DJ, Sanchez-Moran E, Franklin FC, Franklin-Tong VE.** 2015. The *Papaver rhoeas* S determinants confer self-incompatibility to *Arabidopsis thaliana* in planta. *Science* **350**, 684–687.
- Lovy-Wheeler A, Kunkel JG, Allwood EG, Hussey PJ, Hepler PK.** 2006. Oscillatory increases in alkalinity anticipate growth and may regulate actin dynamics in pollen tubes of lily. *The Plant Cell* **18**, 2182–2193.
- Luo N, Yan A, Liu G, et al.** 2017. Exocytosis-coordinated mechanisms for tip growth underlie pollen tube growth guidance. *Nature Communications* **8**, 1687.
- Moseyko N, Feldman LJ.** 2001. Expression of pH-sensitive green fluorescent protein in *Arabidopsis thaliana*. *Plant, Cell & Environment* **24**, 557–563.
- Nagai T, Yamada S, Tominaga T, Ichikawa M, Miyawaki A.** 2004. Expanded dynamic range of fluorescent indicators for  $\text{Ca}^{2+}$  by circularly permuted yellow fluorescent proteins. *Proceedings of the National Academy of Sciences, USA* **101**, 10554–10559.
- Pollard TD.** 2016. Actin and actin-binding proteins. *Cold Spring Harbor Perspectives in Biology* **8**, a018226.
- Poulter NS, Staiger CJ, Rappoport JZ, Franklin-Tong VE.** 2010. Actin-binding proteins implicated in the formation of the punctate actin foci stimulated by the self-incompatibility response in *Papaver*. *Plant Physiology* **152**, 1274–1283.
- Püspöki Z, Storath M, Sage D, Unser M.** 2016. Transforms and operators for directional bioimage analysis: a survey. In: De Vos WH, Munck S, Timmermans JP, eds. *Focus on bio-image informatics*. Cham: Springer International Publishing, 69–93.
- Qin Y, Yang Z.** 2011. Rapid tip growth: insights from pollen tubes. *Seminars in Cell & Developmental Biology* **22**, 816–824.
- Qu X, Jiang Y, Chang M, Liu X, Zhang R, Huang S.** 2015. Organization and regulation of the actin cytoskeleton in the pollen tube. *Frontiers in Plant Science* **5**, 786.
- Rezakhaniha R, Agianniotis A, Schrauwen JT, Griffa A, Sage D, Bouten CV, van de Vosse FN, Unser M, Stergiopoulos N.** 2012. Experimental investigation of collagen waviness and orientation in the arterial adventitia using confocal laser scanning microscopy. *Biomechanics and Modeling in Mechanobiology* **11**, 461–473.
- Riedl J, Crevenna AH, Kessenbrock K, et al.** 2008. Lifeact: a versatile marker to visualize F-actin. *Nature Methods* **5**, 605–607.
- Schindelin J, Arganda-Carreras I, Frise E, et al.** 2012. Fiji: an open-source platform for biological-image analysis. *Nature Methods* **9**, 676–682.
- Smertenko A, Franklin-Tong VE.** 2011. Organisation and regulation of the cytoskeleton in plant programmed cell death. *Cell Death and Differentiation* **18**, 1263–1270.
- Snowman BN, Kovar DR, Shevchenko G, Franklin-Tong VE, Staiger CJ.** 2002. Signal-mediated depolymerization of actin in pollen during the self-incompatibility response. *The Plant Cell* **14**, 2613–2626.
- Staiger CJ, Poulter NS, Henty JL, Franklin-Tong VE, Blanchoin L.** 2010. Regulation of actin dynamics by actin-binding proteins in pollen. *Journal of Experimental Botany* **61**, 1969–1986.
- Sueldo DJ, van der Hoorn RAL.** 2017. Plant life needs cell death, but does plant cell death need Cys proteases? *The FEBS Journal* **284**, 1577–1585.
- Taylor RC, Cullen SP, Martin SJ.** 2008. Apoptosis: controlled demolition at the cellular level. *Nature Reviews. Molecular Cell Biology* **9**, 231–241.
- Thomas SG, Franklin-Tong VE.** 2004. Self-incompatibility triggers programmed cell death in *Papaver* pollen. *Nature* **429**, 305–309.
- Thomas SG, Huang S, Li S, Staiger CJ, Franklin-Tong VE.** 2006. Actin depolymerization is sufficient to induce programmed cell death in self-incompatible pollen. *Journal of Cell Biology* **174**, 221–229.
- Van Damme D, Coutuer S, De Rycke R, Bouget FY, Inzé D, Geelen D.** 2006. Somatic cytokinesis and pollen maturation in *Arabidopsis* depend on TPLATE, which has domains similar to coat proteins. *The Plant Cell* **18**, 3502–3518.
- Van Damme D, Gadeyne A, Vanstraelen M, Inzé D, Van Montagu MC, De Jaeger G, Russinova E, Geelen D.** 2011. Adaptin-like protein TPLATE and clathrin recruitment during plant somatic cytokinesis occurs via two distinct pathways. *Proceedings of the National Academy of Sciences, USA* **108**, 615–620.
- Wang L, Lin Z, Triviño M, Nowack MK, Franklin-Tong VE, Bosch M.** 2019. Self-incompatibility in *Papaver* pollen: programmed cell death in an acidic environment. *Journal of Experimental Botany* **70**, 2113–2123.
- Wilkins KA, Bancroft J, Bosch M, Ings J, Smirnov N, Franklin-Tong VE.** 2011. Reactive oxygen species and nitric oxide mediate actin reorganization and programmed cell death in the self-incompatibility response of *Papaver*. *Plant Physiology* **156**, 404–416.
- Wilkins KA, Bosch M, Haque T, Teng N, Poulter NS, Franklin-Tong VE.** 2015. Self-incompatibility-induced programmed cell death in field poppy pollen involves dramatic acidification of the incompatible pollen tube cytosol. *Plant Physiology* **167**, 766–779.
- Wilkins KA, Poulter NS, Franklin-Tong VE.** 2014. Taking one for the team: self-recognition and cell suicide in pollen. *Journal of Experimental Botany* **65**, 1331–1342.
- Wu J, Wang S, Gu Y, Zhang S, Publicover SJ, Franklin-Tong VE.** 2011. Self-incompatibility in *Papaver rhoeas* activates nonspecific cation conductance permeable to  $\text{Ca}^{2+}$  and  $\text{K}^{+}$ . *Plant Physiology* **155**, 963–973.
- Yang Z.** 2008. Cell polarity signaling in *Arabidopsis*. *Annual Review of Cell and Developmental Biology* **24**, 551–575.
- Zhang L, Xing J, Lin J.** 2019. At the intersection of exocytosis and endocytosis in plants. *New Phytologist* **224**, 1479–1489.
- Zheng Y, Xie Y, Jiang Y, Qu X, Huang S.** 2013. *Arabidopsis* actin-depolymerizing factor7 severs actin filaments and regulates actin cable turnover to promote normal pollen tube growth. *The Plant Cell* **25**, 3405–3423.